Supporting information

Construction of Cu-based MOFs with enhanced hydrogenation performance by integrating open electropositive metal sites

Xiuling Zhang,[a]† Longlong Geng,*[a]† Yong-Zheng Zhang,[a] Da-Shuai Zhang,*[a] Ranhui Zhang,[a] Junna Fu,[a] Jun Gao,[b] Jesse C. Carozza,[c] Zheng Zhou [c] and Haixiang Han*[d]

[a] College of Chemistry and Chemical Engineering, De Zhou University, DeZhou, P. R. China. E-mail: llgeng@126.com; dashuai_74@163.com.

[b] College of Chemical and Environmental Engineering, Shandong University of Science and Technology, Qingdao, P. R. China.

[c] Department of Chemistry, University at Albany, State University of New York, Albany, NY 12222, USA.

[d] Department of Materials Science and Engineering, Cornell University, Ithaca, NY 14853 E-mail: hh685@cornell.edu

† These authors contributed equally to this work.

Table of Contents

I. Experimental Details

Materials

All the starting materials of analytical grade were commercially available and used as received without further purification.

Synthesis of $[Cu_2(L^1)_2 \cdot (DMF)_2]_n$ (1)

A mixture of $Cu(NO_3)_2 \cdot 3H_2O$ (0.08 mmol, 20 mg), 2-nitrobiphenyl-2,4'-dicarboxylic acid (L^1) (0.02 mmol, 6 mg) in 2 mL N,N′-dimethylformamide (DMF) and 2 mL distilled water were sealed in a 20 mL sealed glass vial. The vial was placed in an oven at 100 ºC for 72 h. After cooling to room temperature, blue block crystals were collected by filtration and washed with DMF and H_2O (Yield was 36.6%, based on L^1). Anal. Calcd for $C_{28}H_{18}Cu_2N_2O_{14}$(%): C, 45.84; H, 2.46; N, 3.82. Found: C, 45.85; H, 2.43; N, 3.83. IR (KBr, cm^{-1}): 3430(s), 1667(w), 1663(s), 1558(w), 1527(m), 1406(s), 1351(m), 1103(w), 721(w), 418(m). The activated samples were obtained by exchanging the solvent in the as-synthesized **1** with CH_3OH, followed by evacuation under high vacuum at 200 ºC for 2 h to produce the activated **1** (**1a**).

Synthesis of $[Cu(L^2)(dpye)]_n$ (2)

$Cu(NO_3)_2 \cdot 3H_2O$ (0.08 mmol, 20 mg), 2-nitrobiphenyl-3,4'-dicarboxylic acid (L^2) (0.02 mmol, 6 mg) and 1,2-di(pyridin-4-yl)ethane (dpye) (0.02 mmol, 5 mg) were added to a mixed solvent of N,N′-dimethylacetamide (DMA)/H_2O (v/v =1 : 1, 2 mL) with two drops of tetrafluoroboric acid (HBF$_4$, 56%) in a sealed glass vial. Then, the obtained mixture was ultrasonicated to dissolve and then heated at 100 °C for 72 h. After cooling to room temperature, blue block crystals were collected by filtration and washed with DMA and H_2O (Yield: 33.5% based on L^2). Elemental anal. Calcd for $C_{26}H_{17}Cu_2N_3O_6$ (%): C, 58.81; H, 3.22; N, 7.91. Found: C, 58.83; H, 3.21; N, 7.90. IR (KBr, cm^{-1}): 3424(s), 2926(m), 1609(m), 1578(w), 1410(m), 1369(w), 1241(s), 1103(s), 777(s), 730(m), 662(s), 494(s).

X-ray Characterizations

The single-crystal diffraction data of **1** and **2** were collected in a Rigaku Supernova CCD diffractometer equipped with a mirror-monochromatic enhanced Cu-Kα radiation (λ = 1.54184 Å). The dataset was corrected by empirical absorption correction using spherical harmonics, implemented in the SCALE3 ABSPACK scaling algorithm. [1] The structure dates solved and refined by direct methods and full-matrix least-squares methods using the SHEXL-2014. [2] The integrated system of single suite Olex2 was used for the crystallographic programs. [3] All non-hydrogen atoms were refined anisotropically. The hydrogen atoms were implemented by geometrically calculations, and their positions and thermal parameters, during the structure refinement of them, were fixed as well. The summarized crystallographic data are showed in Table S1. The relevant bond lengths and angles are listed in Table S2 and S3. The contribution of disordered solvent molecules was treated using the SQUEEZE procedure implemented in PLATON.[4]

Powder X-ray diffraction (PXRD) data of the Co-MOF were recorded on a Bruker D8A A25 X-ray diffractometer (Cu-Ka radiation, λ=0.1542 nm), with 2θ range from 5-50° at room temperature. XPS was performed on a Thermo ESCA LAB 250 system with MgKa source (1254.6 eV). Under nitrogen protection, the thermogravimetric analyses (TGA) data were performed by SHIMADZU DTG-60 thermo analyzer from 30 ℃ to 700 ℃ with a heating rate of 10 ℃·min^{-1}.

Catalytic Measurements

The catalytic hydrogenation of 4-NP was selected as a model reaction using $NaBH_4$ as reducing agent in this experiment. In a typical experiment, 20.0 mL of fresh $NaBH_4$ solution (0.1 M) was mixed with 20.0 mL of 4-NP solution (0.4 mM) in a conical flask at room temperature. The color of the solution clearly changes from light yellow to yellow-green immediately. Then, 2.0 mg of the as-prepared catalyst was added to the mixture and the solution color changed gradually from yellow to colorless. UV-Vis spectroscopy was used to record the change in absorbance at a time at $\lambda = 400$ nm. The conversion of 4-NP was calculated using $(A_0-A_t)/A_0$, where A_t and A_0 represent the absorbance at the intervals and the initial stage of 4-NP, respectively.

The leaching experiment was carried out as follows: after 3 min of reaction, the solid catalysts were separated with a Buchner funnel. Then, the mixture of the filtrate was put into the reactor and continuously reacted under the same conditions without any solid catalyst. In the recycle test, the absorbance of the solution was tested after reaction for 7 min. The catalyst was separated from the solution by centrifugation and rinsed with water after reaction and was reused in the next reaction. Eight repeat experiments were carried out with the same procedure.

II.   Characterization Results

Table S1 Crystal data and structure refinement parameters for **1** and **2**.

Compound	1	2
Chemical formula	$C_{34}H_{28}Cu_2N_4O_{14}$	$C_{30}H_{26}CuN_4O_7$
M_r	843.68	618.09
Temperature (K)	173(2)	173(2)
Wavelength (Å)	1.54178	1.54178
Crystal system	Orthorhombic	Triclinic
Space group	$Pbca$	$P-1$
a (Å)	16.2198(2)	10.0881(2)
b (Å)	10.5608(1)	10.2574(2)
c (Å)	21.3159(2)	14.2782(3)
α (°)	90	76.988(2)
β (°)	90	72.988(2)
γ (°)	90	82.528(2)
V (Å^3)	3651.29(7)	1373.28(5)
Z	4	2
$F(000)$	1720	638
μ (mm^{-1})	2.077	1.603
ρ_{calcd} (g·cm^{-3})	1.535	1.495
Crystal size (mm)	0.12×0.08×0.04	0.10×0.06×0.03
Transmission factors (min/max)	0.789, 0.922	0.856, 0.953
Reflections collected	11489	24082
Independent reflections	3230	4346
R_{int}	0.0232	0.0292
θ range (°) for data collection	4.15–72.45	3.31–72.69
$R[F^2 > 2\sigma(F^2)]$, $wR(F^2)$, S	0.0506, 0.1522, 1.092	0.0384, 0.0995, 1.069

[a]$R_1 = \Sigma||F_o|-|F_c||/\Sigma|F_o|$. [b]$wR_2 = [\Sigma[w(F_o^2-F_c^2)^2]/\Sigma[w(F_o^2)^2]]$.

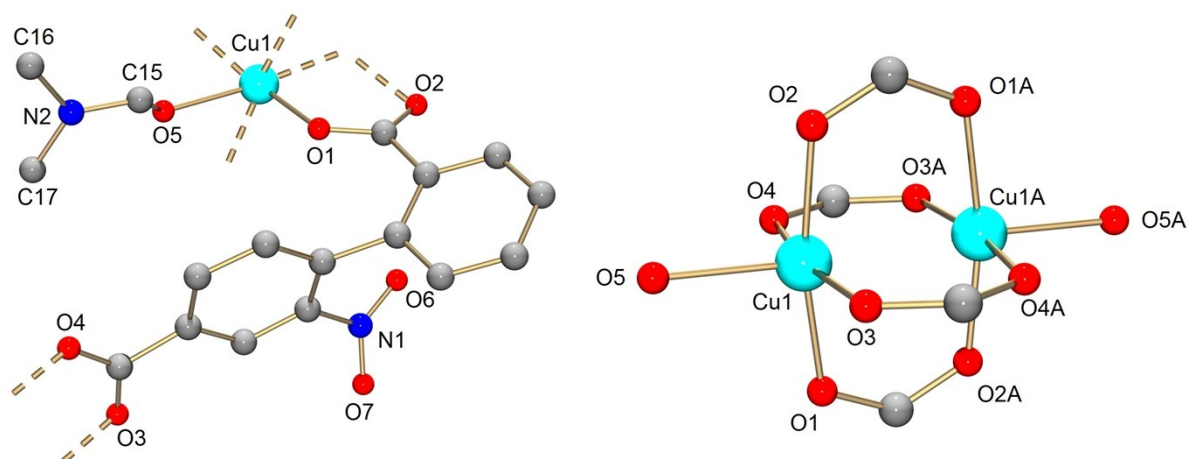[c]Quality-of-fit = $[\Sigma[w(F_o^2-F_c^2)^2]/(N_{obs}-N_{params})]^{1/2}$, based on all data.

Fig. S1 Asymmetric unit of compound **1** (left) and coordination environment of Cu²⁺ in compound **1** (right), ball-and-stick model. H atoms are omitted for clarity. Color scheme: green, copper; red, oxygen; blue, nitrogen; gray, carbon.

Table S2. Selected bond distances (Å) and bond angles (°) in compound **1**.

Bond Name	Distance	Angle Name	Angle
Cu1–Cu1A	2.641(1)	O1–Cu1–O2	168.39(9)
Cu1–O1	1.957(2)	O1–Cu1–O3	90.27(10)
Cu1–O2	1.961(2)	O1–Cu1–O4	88.34(10)
Cu1–O3	1.983(2)	O1–Cu1–O5	95.49(10)
Cu1–O4	1.961(2)	O2–Cu1–O3	88.96(10)
Cu1–O5	2.101(13)	O2–Cu1–O4	90.10(10)
Cu1–O5X	2.141(12)	O2–Cu1–O5	96.14(6)
		O3–Cu1–O4	168.48(10)
		O3–Cu1–O5	93.11(10)
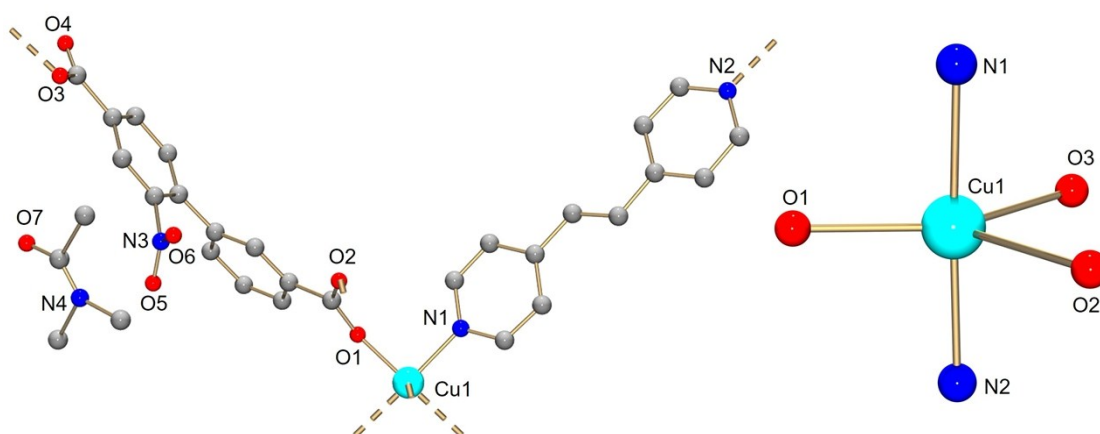
Fig. S2 Asymmetric unit of compound **2** (left) and coordination environment of Cu²⁺ in compound **2** (right), ball-and-stick model. H atoms are omitted for clarity. Color scheme: green, copper; red, oxygen; blue, nitrogen; gray, carbon.

Table S3. Selected bond distances (Å) and bond angles (°) in compound **2**.

Bond Name	Distance	Angle Name	Angle
Cu1–O1	1.954(2)	O1–Cu1–O2	123.50(7)
Cu1–O2	2.268(2)	O1–Cu1–O3	148.96(7)
Cu1–O3	1.991(2)	O2–Cu1–O3	87.07(5)
Cu1–N1	2.022(2)	N1–Cu1–O1	93.34(7)
Cu1–N2	2.032(2)	N1–Cu1–O2	88.34(7)
		N1–Cu1–O3	92.79(7)
		N2–Cu1–O1	88.41(7)
		N2–Cu1–O2	87.25(7)
		N2–Cu1–O3	87.82(7)
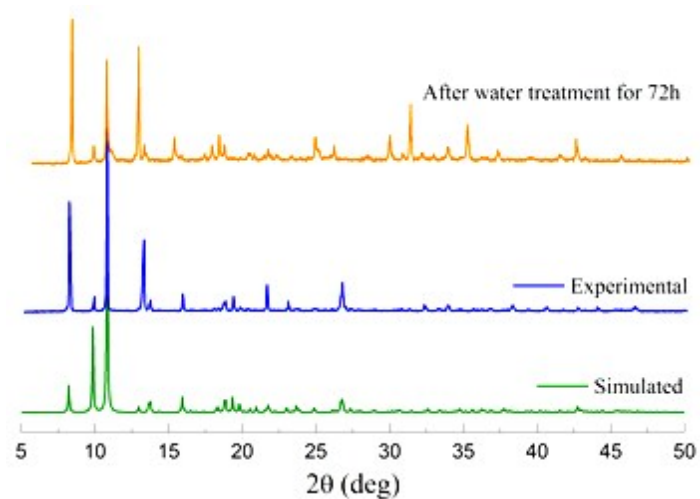
Fig. S3 X-ray powder diffraction patterns of compound **1** and after being treated under different conditions for 72 h (Simulated pattern derived from the X-ray single crystal data).
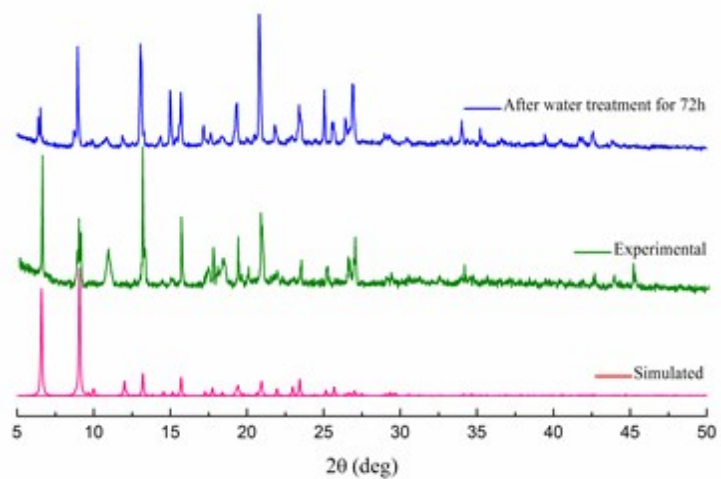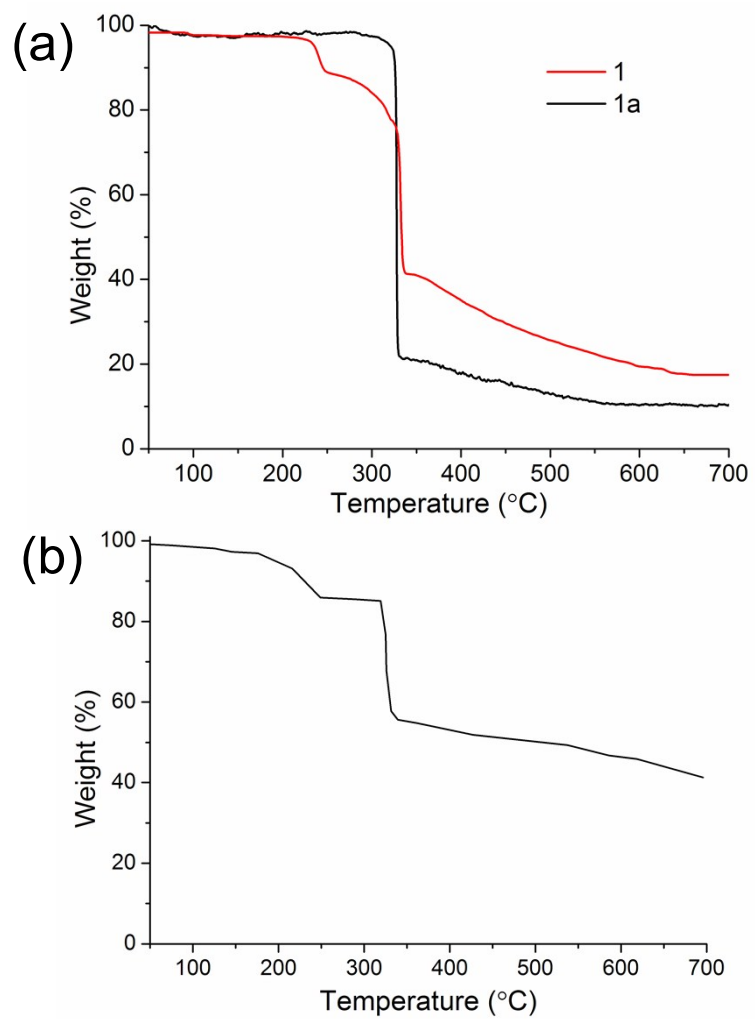
Fig. S4 X-ray powder diffraction patterns of compound **2** and after being treated under different conditions for 72 h (Simulated pattern derived from the X-ray single crystal data).

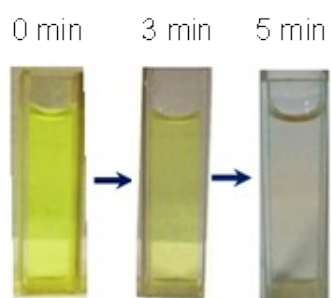**Fig. S5** TGA experiments of compound **1** and compound **1a** (a) and compound **2** (b).

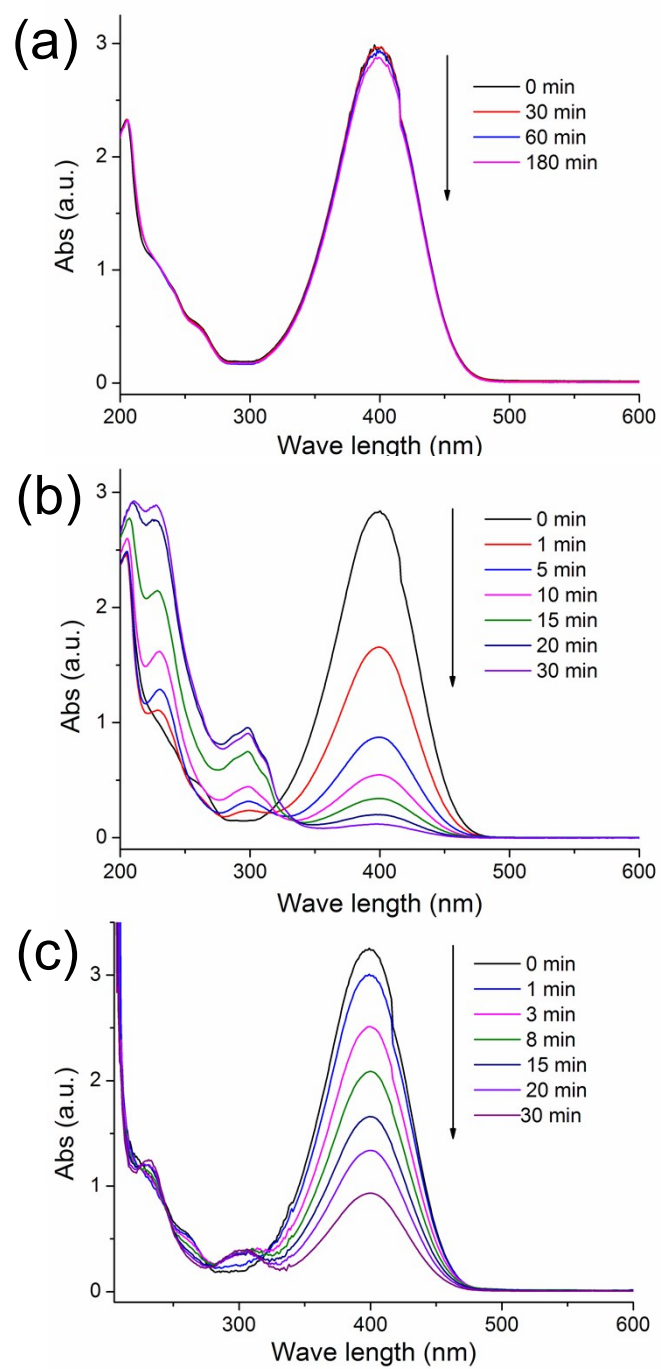**Fig. S6** Color change of the hydrogenation of 4-NP in the presence of compound **1**.

Fig. S7 UV-Vis spectra of the hydrogenation of 4-NP without any catalysts (a) and in the presence of compound **2** (b) and CuO NPs (c).

Table S4. Catalytic performance of different catalysts in the catalytic hydrogenation of 4-NP.

Catalysts	Time (s)	$k \times 10^{-3}$ (s^{-1})	Ref
Pd /Ni-CeO$_{2-x}$	100	47.9	5
Ag-Ni/RGO	60	48.4	6
Au-Ag/GO	30	142.7	7
Pd /Fe$_3$O$_4$@CeO$_2$	180	21.5	8
Cu/Ag NPs	240	3.95	9
NiCoO$_x$/RGO	1800	1.55	10
Fe$_3$O$_4$	640	1.06	11[b]
Ni-1	1200	2.93	12
CoO$_x$/CN	600	4.20	13
Co-MOF	1800	1.20	14
MOF (**1**)	300	**14.20**	This work
MOF (**2**)	1800	1.70	This work
CuO NPs	1800	0.85	This work

[a] Rate constant k normalized to the amount of metal species

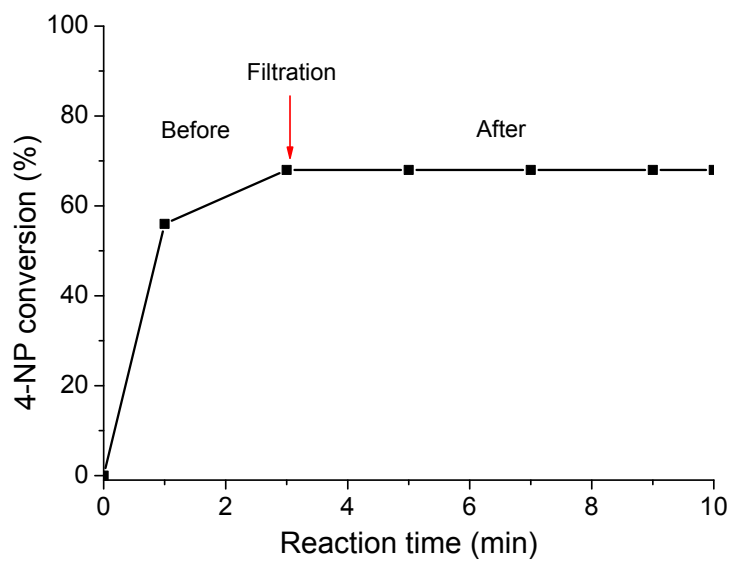[b] Hydrazine as reductant and NaOH as assistant.

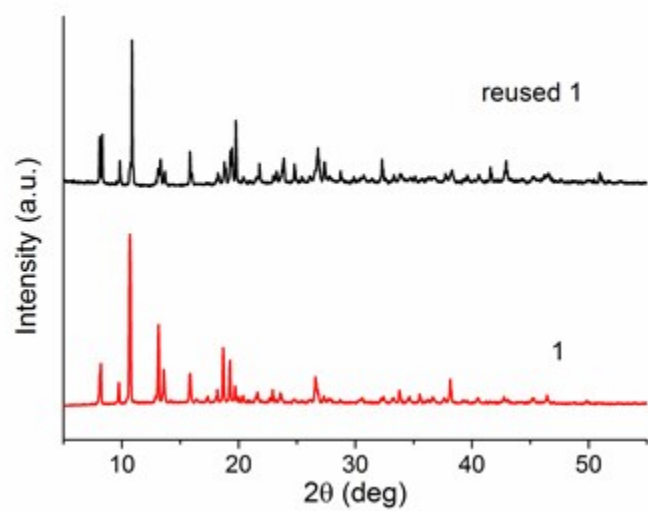**Fig. S8** Leaching experiment of filtered compound **1** during hydrogenation.

Fig. S9 X-ray powder diffraction pattern comparison of compound **1** and regenerated compound **1** after reaction.
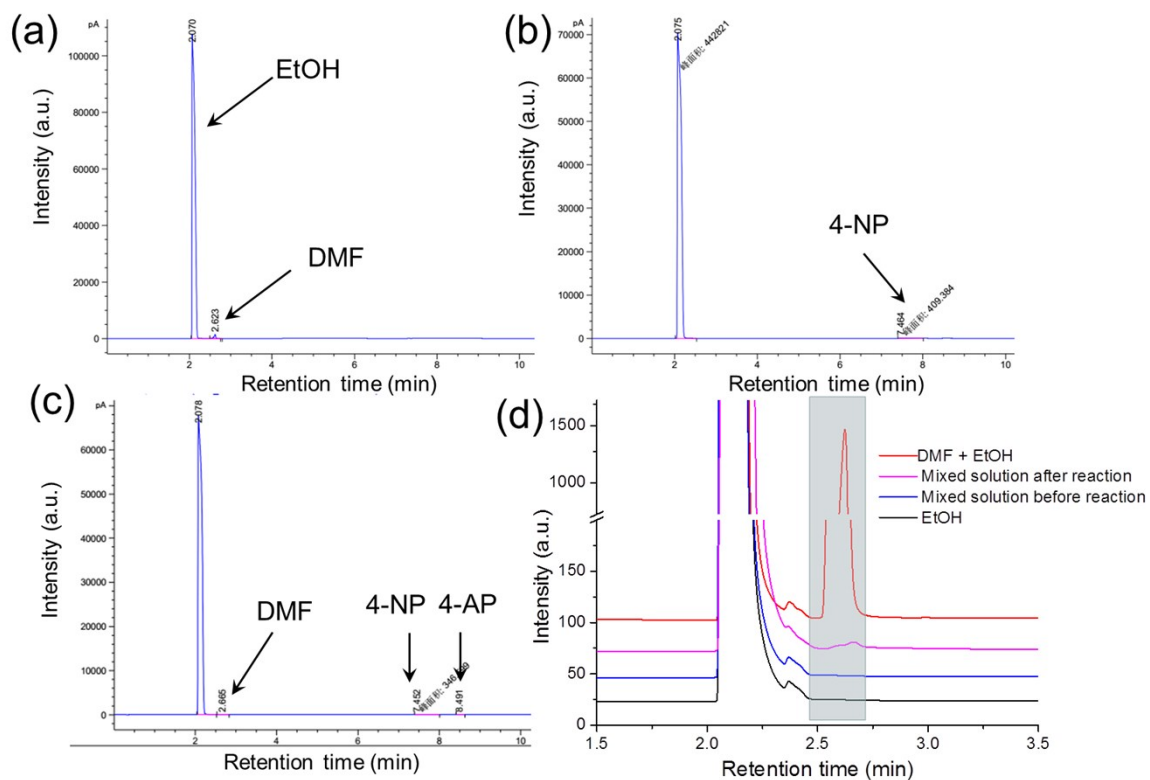
Fig. S10 GC spectra of DMF dispersed in EtOH solution (a), mixed solution before catalytic reaction (b), mixed solution after catalytic reaction (c) and high resolution GC spectra of different solutions (d).
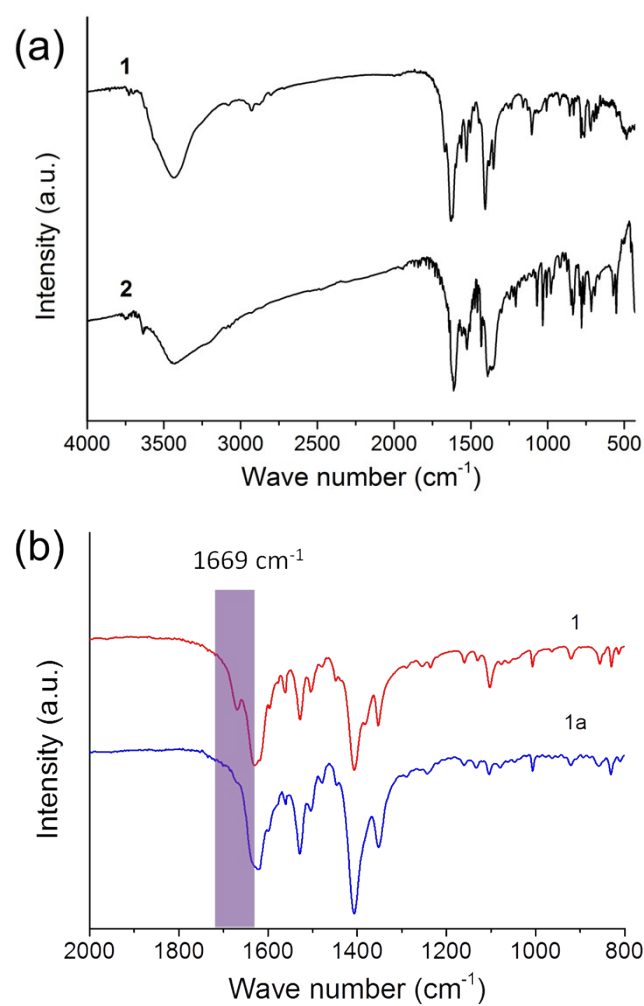
Fig. S11 FTIR spectra of compound **1** and compound **2** (a) and **1a** (b).

From the FTIR spectra of 1 and 1a, the intensity of the characteristic peak corresponding to C=O stretching vibration (1669 cm^{-1}) from amide group of DMF decreased or even disappeared after activation, indicating the removal of DMF during activation treatment, which is in agreement with the TG results.
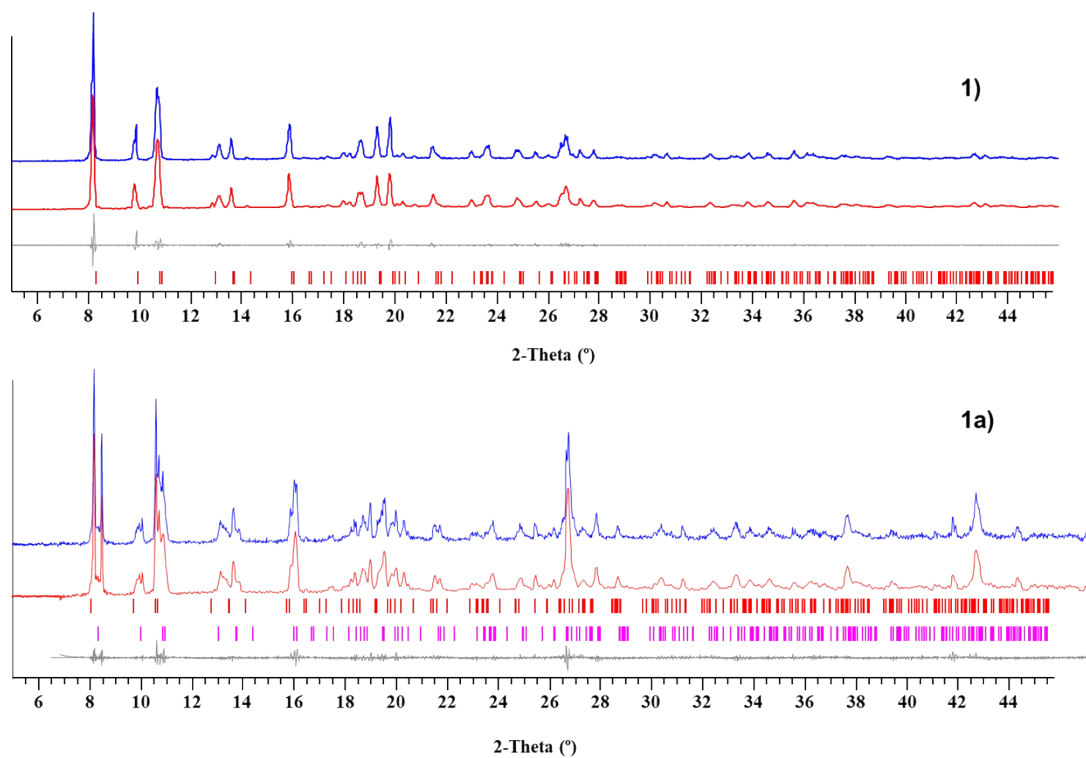
Fig. S12 The X-ray powder diffraction pattern and LaBail profile fit of compound **1** before activation (Blue and red lines are experimental and calculated patterns, respectively. Grey is the difference curve with theoretical positions shown at the bottom) and the X-ray powder diffraction pattern and LaBail profile fit of the actived compound **1** (**1a**). Blue and Red lines are experimental and calculated patterns, respectively. Grey is the difference curve with theoretical positions from two different phases (red-phase 1, purple-phase 2) shown at the bottom.

Table S5. Unit cell parameters calculated from LaBail profile fit for the powder diffraction patterns.

Compound	**1**	**1a**	
Phase	Phase 1	Phase 1	Phase 2
Space Group	*Pbca*	*Pbca*	*Pbca*
a(Å)	16.2623(2)	16.2617(2)	15.2580(2)
b(Å)	10.5952(2)	10.5950(2)	10.5773(3)
c(Å)	21.3216(2)	21.3208(2)	21.3155(2)
V(Å^3)	3673.7(3)	3670.9(3)	3440.1(4)

The LaBail profile simulations of the X-ray diffraction patterns reveal that compound **1** before activation has a single phase that matches well to the calculated pattern based on X-ray single crystal data, while the activating process results in a phase splitting with two different phases appearing in the X-ray powder diffraction spectrum (Fig. S12). LaBail fit indicates both phases belong to the same space group but featuring different unit cell parameters. Phase 1 has very close unit cell parameters to that before activation whereas the calculated unit cell parameters of phase 2 display an obvious volume contraction. The above results implied that a fraction of bulk materials lose their DMF molecules but maintaining the complete 2D framework during the degas process.
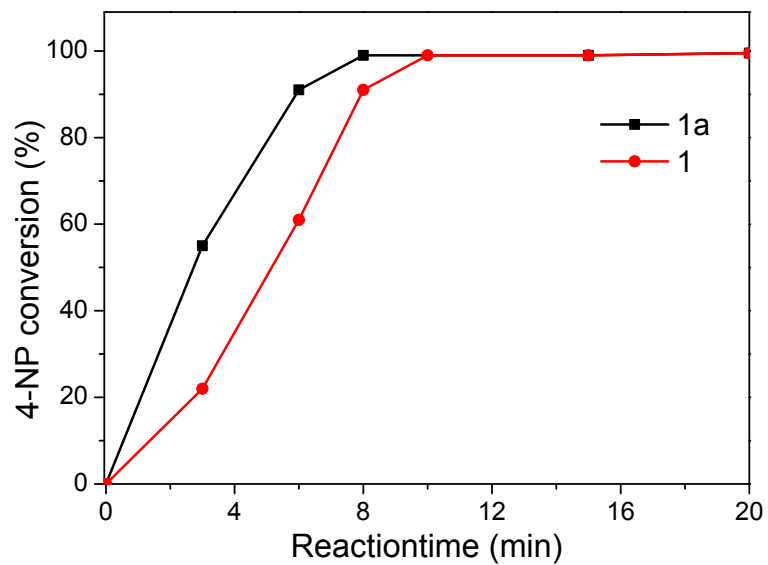
Fig. S13 Catalytic performance of compound **1** and compound **1a** in the hydrogenation of 4-NP. Reaction conditions: 40.0 mL of 4-NP solution (0.4 mM) and 40.0 mL of fresh $NaBH_4$ solution (0.1 M), catalyst 2 mg, 25 ºC, 1atm.

III. References

[1] Oxford Diffraction, CrysAlis Pro software, 2010, Ver. 1.171.34, Yarnton, Oxfordshire. Oxford Diffraction Ltd.

[2] G. M. Sheldrick, SHELXTL NT Version 5.1. Program for Solution and Refinement of Crystal Structures (University of Göttingen, Germany, 1997, 246.

[3] L. J. Farrugia, J. Appl. Crystallogr. 1999, **32**, 837.

[4] A. L. Spek, Acta Crystallogr., Sect. D: Biol. Crystallogr.,2009, **2**, 148.

[5] Y. F. Jiang, C. Z. Yuan, X. Xie, X. Zhou, N. Jiang, X. Wang, M. Imran, A. W. Xu, *ACS Appl. Mater. Interf.*, 2017, **9**, 9756-9762.

[6] R. Dhanda, M. Kidwai, *J. Mater. Chem. A,* 2015, **3**, 19563-19574.

[7] T. Wu, L. Zhang, J. Gao, Y. Liu, C. Gao, J. Yan, *J. Mater. Chem. A*, 2013, **1**, 7384-7390.

[8] Q. Wang, Y. Li, B. Liu, Q. Dong, G. Xu, L. Zhang, J. Zhang, *J. Mater. Chem. A*, 2015, **3**, 139-147.

[9] W. Wu, M. Lei, S. Yang, L. Zhou, L. Liu, X. Xiao, C. Jiang, V. Roy, *J. Mater. Chem. A*, 2015, **3**, 3450-3455.

[10] S. Bai, X. Shen, G. Zhu, M. Li, H. Xi, K. Chen, *ACS Appl. Mater. Interf.*, 2012, **4**, 2378-2386.

[11] H. Li, J.Y. Liao, X.B. Zhang, *J. Mater. Chem. A*, 2014, **2**, 17530-17535.

[12] Y. Z. Li, Y.L. Cao, D. Z. Jia, *J. Mater. Chem. A*, 2014, **2**, 3761-3765.

[13] X. Zhang, N. Wang, L. Geng, J. Fu, H. Hu, D.-S. Zhang, B. Zhu, J. Carozza, H. Han, J. Colloid Interf. Sci, 2018, **512**, 844-852.

[14] X. Zhang, J. Fu, D.-S. Zhang, L. Geng, Polyhedron, 2018, **146**, 12-18.